Memoirs of the Faculty of Science, Kyoto University, Series of Physics, Astrophysics, Geophysics and Chemistry, Vol. XXXIX, No. 2, Article 1, 1995

A Borehole Stress-strain Measurement System by Employing Electronic Speckle Pattern Interferometry

By

Jun HIRABAYASHI* and Shuzo TAKEMOTO

Department of Geophysics, Faculty of Science, Kyoto University
Kyoto 606-01, Japan

(Received November 17, 1994)

Abstract

A borehole stress-strain measurement system based on Electronic Speckle Pattern Interferometry (ESPI) was developed and employed for measuring crustal stresses and strains. The system was designed to be small in size and light in weight, and to be able to measure quantitatively out-of-plane deformations (radial deformations) of the cylindrical area in a borehole in terms of a wavelength of the laser light. Laboratoy tests confirmed that the system could be available for precise stress-strain measurements. We have carried out field experiments employing the system at Hiraki mine in Hyogo Prefecture. As a result, some problems to be solved for employing the system in field experiments have been clarified. Based on these experiments, a measurement module has been improved to measure out-of-plane displacements not only in the surrounding cylindrical area but in the bottom area. It will also be possible to measure in-plane displacements in both side and bottom areas of a borehole by modifying an optical arrangement of the module. Using a new system, laboratory tests were performed. Consequently, it was confirmed that the new system was able to measure quantitatively a small deformation of the object in terms of fringe displacements in speckle patterns. However, there remain some problems to be solved to apply the system for measurements of crustal deformation in boreholes: that is, the waterproof design of the system and the introduction of the small semi-conductor laser source instead of the He-Ne gas laser and optical fiber system used in this study. As another application of the ESPI system in geophysical sciences, we propose to employ it in precise measurements of tunnel deformation.

Contents

* Present address: Canon Co., Ltd., Shimomaruko 3-30-2, Ota-ku, Tokyo 146, Japan.

1. Introduction

Knowledge of the state of crustal stresses and strains plays an important role in understanding the driving mechanism of tectonic processes. It is also important to know their regional distributions as well as time variations to promote earthquake prediction studies. Stress measurements have thus been carried out in various regions in Japan (e.g., TANAKA, 1987; TANAKA et al., 1990).

Methods to measure crustal stresses are classified into the hydrofracturing method, the stress-relief method by using strain-gauges, the breakout method and so on (KAMEOKA, 1978). The hydrofracturing method can determine the state of crustal stress from fractures which appear in a borehole wall due to a hydropressure. In case of the stress-relief method, the crustal stress is determined from measurements of deformation of a borehole when the stress is relieved by means of overcoring. Deformation measurements are combined with the elastic property of rocks to estimate the state of stresses. The radial deformation of a borehole is usually measured by determining a crustal stress tensor. In some cases, the crustal stress tensor is determined by measuring the deformation of the bottom of the borehole. A device using a 16 element-gauge was developed for such a purpose (OKA et al., 1979). In the breakout method, directions of a principal stress are determined from breakouts that are zones of spalling and fracturing appeared on side walls of a borehole (e.g., MASTIN, 1988).

A unique instrument for measuring *in situ* stress fields in crustal rocks was developed by a group at the California Institute of Technology (BASS et al., 1986). The instrument is called a 'holographic stressmeter' and is able to measure a small displacement around a borehole in terms of an interference fringe pattern on a hologram. The state of stress fields around the borehole can be determined by the same procedure as that commonly used in the stress-relief method.

On the other hand, extensometers, which employ length standards in forms of quartz tubes or super-invar bars, have been widely used in many observatories to search for crustal deformations. If we measure tidal strains on an order of 10^{-8} by means of an extensometer, relative displacements between the fixed and free ends of an extensometer with a length of 10 m are found to be 0.1 μm or so. A resolution of 1×10^{-10} is required to observe tidal strains with a precision of 1%. As for the other devices, crustal strain measurements using resistive strain gauges (YANAGISAWA, 1984) and multi-component small borehole strainmeters (ISHII et al., 1992) have been reported.

In any case, absolute calibration of these instruments is difficult. One solution to overcome this difficulty is the use of laser extensometers which can measure small strains quantitatively in terms of the wavelength of light (TAKEMOTO, 1979). As mentioned above, optical interferometric devices have been effectively used in stress and strain measurements in geophysical sciences. We thus intend to improve the interferometric measurement system of crustal stress and strain.

Among the optical interferometric methods, Speckle Pattern Interferometry (SPI) is a technique that can measure the small deformation of an object without touching it in terms of the wavelength of the laser light. The speckle pattern is caused by the

random interference of scattered waves from a diffusely reflecting surface of an object. SPI which uses photographs as recording devices involves difficulties in continuously automatic operation.

Electronic Speckle Pattern Interferometry (ESPI), which obtains images by using electronic devices such as a video camera and an image-processor, was developed in the 1970's and has been applied to various purposes since then. As an example of a practical application of ESPI to laboratory mesurements of small displacements, YAMAGUCHI (1981) developed a laser speckle strain gauge. In solid earth sciences, laser speckle interferometry is used to study the process of the fracture zone in rocks (CHENGYONG et al., 1990).

The applicability of ESPI to crustal stress and strain measurements is described in this paper. First, design and construction of the ESPI borehole measurement system is described. Secoond, problems to be solved through laboratory tests and field experiments are clarfied.

2. Design and Construction of an ESPI Stress-strain Measurement System

2.1. Procedure of Crustal Stress Measurement by Strain-relief Method

The principle of measurements of crustal stress by means of the strain-relief (overcoring) method is illustrated in Figure 1. A rock mass is first assumed to be subjected to two dimensional stresses . A pilot hole is drilled into the rock at the point where the stress should be measured. After the drilling, the hole should be deformed by the pre-existing crustal stress. The measurement module of the system is then attached in the borehole. The borehole is sealed by means of a borehole plug to waterproof the system. Then the pilot borehole is overcored and separated from the surrounding rock mass. As a result, radial displacements of the pilot borehole should be measured. Crustal stresses in rocks, in which the measurement module is set up, can be determined from the resultant displacements, if elastic properties of rocks are known.

The present system is designed to measure the radial displacements of the borehole wall (cylindrical area whose height is 5 cm). The system is required to have not only high accuracy but mobility.

2.2. Analysis of Elastic Deformations

In Japan, early contribution to analyze the relation between a radial displacement of a circular borehole and a crustal stress was made by HIRAMATSU and OKA (1962). An analysis of elastic deformations by numerical calculations is described in the following.

One of the coordinate systems referred to in this analysis has the z-axis along the borehole axis (positive in the forward direction of boring) and the x- and y-axes perpendicular to the z-axis to form a right-handed system. Another system using cylindrical coordinates (r, θ, z) with the z-axis coincident with that of the Cartesian coordinates is introduced and θ is measured from the x-axis. The rock is assumed to be isotropic. If we denote components of stress tensors by σ_x, σ_y, σ_z, τ_{yz}, τ_{zx} and τ_{xy},

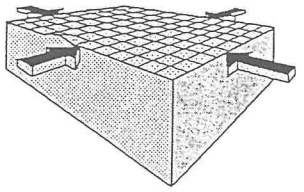

(a) A rock mass subjected to the horizontal stresses.

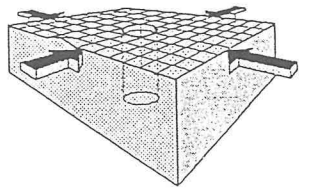

(b) A pilot hole drilled into the rock to the point where the stress in the rock should be measured.

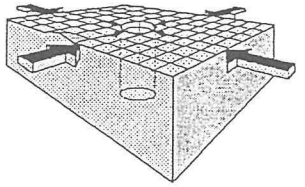

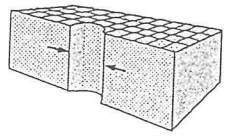

(c) Deformations of the hole after drilling.

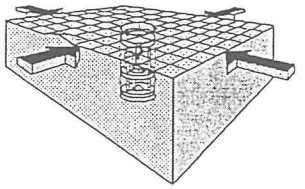

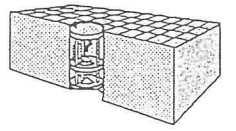

(d) After the measurement module of the system is fixed, the pilot borehole is sealed by means of a borehole plug for the purpose of waterproof.

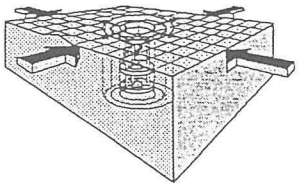

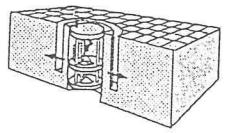

(e) Radial displacements of the pilot borehole to be measured.

Fig. 1. Principle of crustal stress measurements by overcoring.

a radial displacement d_r is given by the following form,

$$d_r=\frac{2r_0}{E}(f_1\ f_2\ f_3\ f_4)\begin{pmatrix}\sigma_x\\ \sigma_y\\ \tau_{xy}\\ \sigma_z\end{pmatrix}, \tag{1}$$

where, r_0 is the radius of the borehole, E is the Young's modulus, ν is the Poisson's ratio, and,

$$f_1=(1-\nu^2)(1+2\cos 2\theta)+\nu^2, \tag{2}$$
$$f_2=(1-\nu^2)(1-2\cos 2\theta)+\nu^2, \tag{3}$$
$$f_3=4(1-\nu^2)\sin 2\theta, \quad \text{and,} \tag{4}$$
$$f_4=-\nu. \tag{5}$$

Equation (1) shows that three measurements in independent directions are required at least to determine the whole stress tensors.

2.3. Construction of the ESPI Measurement System

Figure 2 shows a schematic diagram of the measurement module of the crustal stress measurement system employing electronic speckle pattern interferometry. The height of the measurement module is 40 cm and its diameter is 10 cm. The weight of the module is about 5 kg. The module is fixed by three legs (J) at the upper side of the module as well as by three legs (J) near the bottom. The legs are able to be expanded and tightly contract to the borehole wall by compressed air.

The laser beam is supplied from a He-Ne laser of 15 mW and fed to a beam expander (A) through an optical fiber (1), and then split by a beam splitter (B) to two waves ; one is the reference wave toward a reference plane (C) and the other is the object wave toward a borehole wall (G). The object wave is distributed in all directions (360°) surrouding the borehole wall by a cone mirror (F). Two waves reflected by both the object wall and the reference plane interfere with each other, and the interference image is recorded by a video camera (H). Speckle patterns arise in the images. The speckle pattern is caused by the random interference of scattered waves from the surface of a diffusing object and reference plane illuminated by the coherent light of the laser. The images obtained are processed by a personal computer (NEC PC9801VX) and

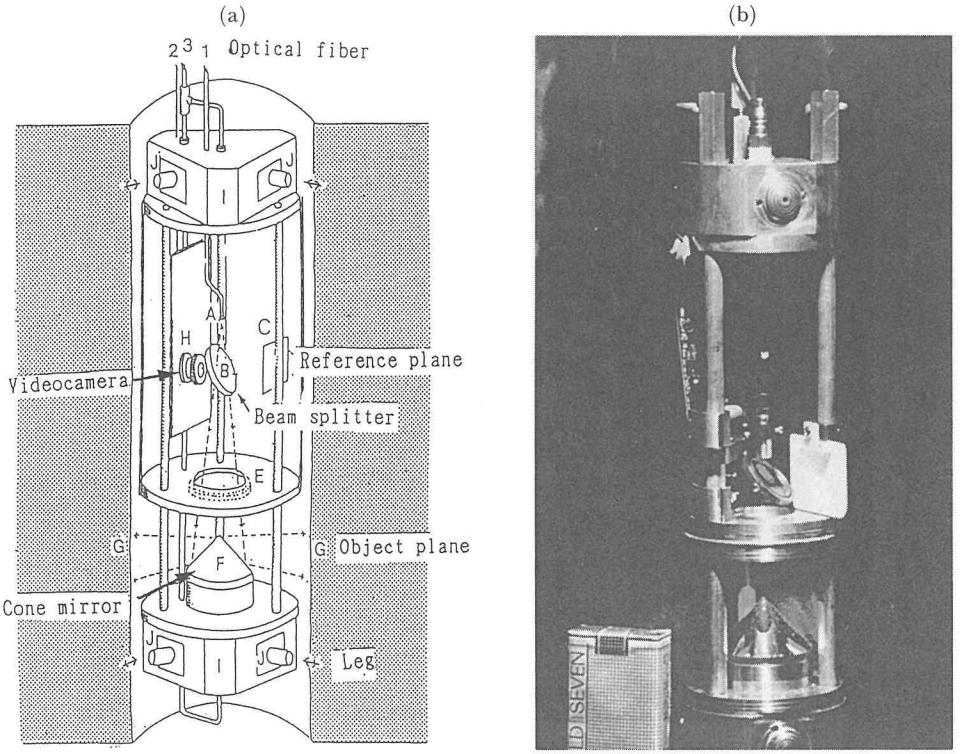

Fig. 2. (a) Schematic diagram of the borehole module of the ESPI stress measurement system. (b) View of the borehole module.

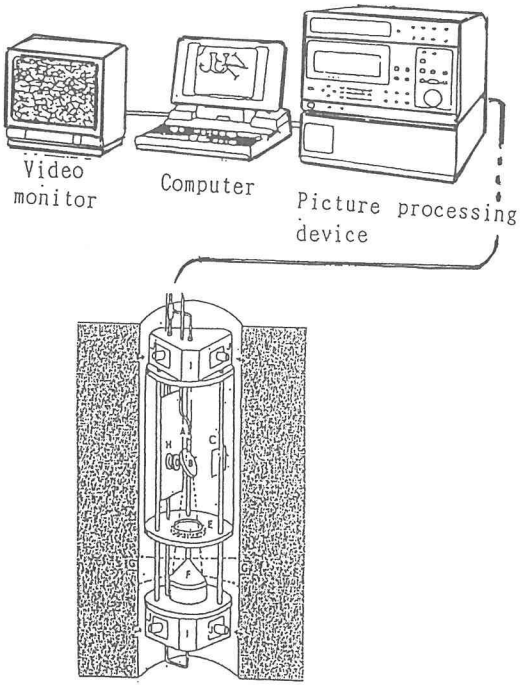

Fig. 3. Setup of the ESPI stress measurement system.

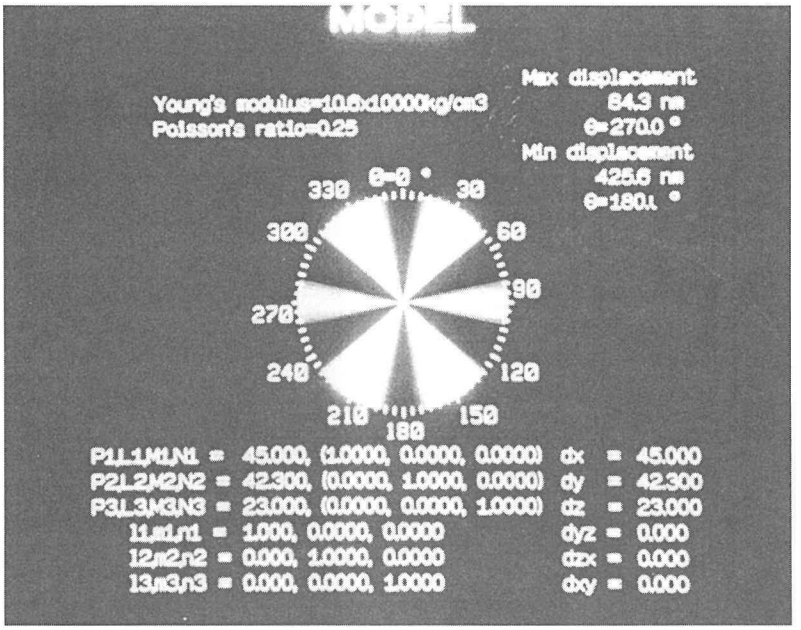

Fig. 4. An example of estimation of radial displacements which should be detected by the measurement system.

an image processor (EDEC IMAGE-MAX). The radial displacement of the borehole wall can be estimated by the image processing in terms of a half of the wavelength of the laser light. The video camera is a KM-30 image sensor camera unit in which CCD has 512×582 pixels. A minimum illumination needed by the camera is 5 lux. The image processor has 512×480 pixels. Therefore, pixels to be processed in the system are 512×480. Figure 3 shows the setup of the whole system.

Figure 4 shows an example of theoretical results for radial expansions. The theoretical image was calculated to represent a stored image after overcoring. Maximum and minimum radial displacements are shown in Figure 4.

2.4. Calculation of ESPI Image in the System

The theory of out-of-plane ESPI (reference light method) measurement by which the out-of-plane deformations are measured is described in this subsection.

Let a coordinate on the CCD and that on the object plane be (x,y) and (X, Y), respectively. (x,y) can be expressed as a function related to (X, Y),

$$(x,y)=f(X, Y). \tag{6}$$

At the point (x,y) on the CCD of the video camera, the object wave $A_o\ (x,y)$ reflected from (X, Y) on the object plane and reference wave $A_r\ (x,y)$ reflected from (X_r, Y_r) are given in the form of the following equations, respectively.

Object wave

$$A_o(x,y)=a_o\ (X, Y, Z_o)\exp\left[ik(\sqrt{X^2+Y^2+(Z_l+Z_o)^2}+\sqrt{X^2+Y^2+(Z_o+Z_c)^2})\right],$$

Reference wave

$$A_r(x,y)=a_r(X_r, Y_r, Z_r)\exp\left[ik(\sqrt{X_r^2+Y_r^2+(Z_l+Z_r)^2}+\sqrt{X_r^2+Y_r^2+(Z_r+Z_c)^2})\right], \tag{7}$$

where,

Z_l : the length of the optical path from the focal point of the fiber lens to the center of the beam splitter,

Z_o : the length of the optical path from the center of the beam splitter to the center of the object plane $(X=0, Y=0)$,

Z_r : the length of the optical path from the center of the beam splitter to the center of the reference plane,

Z_c : the length of the optical path from the center of the beam splitter to the center of the CCD $(x=0, y=0)$,

$a_o\ (X, Y, Z_o)$: the distribution of the light intensity (the object wave),

$a_r\ (X_r, Y_r, Z_r)$: the distribution of the light intensity (the reference wave), and

k : a wave number $(=2\pi/\lambda)$[λ: the wavelength of the laser light].

Using the proportional relation,

$$X : Y : (Z_l+Z_o)=X_r : Y_r : (Z_l+Z_r),$$

X_r and Y_r are expressed by,

$$X_r=\left(\frac{Z_l+Z_r}{Z_l+Z_o}\right)X$$

$$=RX,$$

$$Y_r=\left(\frac{Z_l+Z_r}{Z_l+Z_o}\right)Y$$

$$=RY,$$

where,

$$R=\frac{Z_l+Z_r}{Z_l+Z_o}.$$

Then Equation (7) is transformed into the following form,

$$A_r(x,y)=a_r(X_r, Y_r, Z_r)\cdot\exp\left[ik(R_{lr}+R_{cr})\right], \tag{8}$$

where,

$$R_{lr}=\sqrt{(RX)^2+(RY)^2+(Z_l+Z_r)^2}, \quad \text{and,}$$
$$R_{cr}=\sqrt{(RX)^2+(RY)^2+(Z_r+Z_c)^2}.$$

Since the image intensity $I(x,y)$ on the CCD is given by $|A_o(x,y)+A_r(x,y)|^2$, it is expressed in the follwing form.

$$\begin{aligned}I(x,y)&=|A_o(x,y)+A_r(x,y)|^2\\&=a_o{}^2(X, Y, Z_o)+a_r{}^2(X_r, Y_r, Z_r)\\&\quad+2a_o(X, Y, Z_o)a_r(X_r, Y_r, Z_r)\cdot\cos\left[k((L_1+L_2)-(R_{lr}+R_{cr}))\right],\end{aligned} \tag{9}$$

where,

$$L_1=\sqrt{X^2+Y^2+(Z_l+Z_o)^2}, \quad \text{and,}$$
$$L_2=\sqrt{X^2+Y^2+(Z_o+Z_c)^2}.$$

If the object plane (the borehole wall) is deformed by $(\delta_X, \delta_Y, \delta_Z)$ and k is changed to k', two waves should be changed. Then,

$$\begin{aligned}I'(x,y)&=|A'_o(x,y)+A'_r(x,y)|^2\\&=a^2{}_o(X+\delta_X, Y+\delta_Y, Z_o-\delta_Z)+a^2{}_r(X_r, Y_r, Z_r)\\&\quad+2a_o(X+\delta_X, Y+\delta_Y, Z_o-\delta_Z)a_r(X_r, Y_r, Z_r)\\&\quad\cdot\cos\left[k'((L_1'+L_2')-(R_{lr}+R_{cr}))\right],\end{aligned} \tag{10}$$

where,

$$L_1'=\sqrt{(X+\delta_X)^2+(Y+\delta_Y)^2+(Z_l+Z_o-\delta_Z)^2}, \quad \text{and,}$$
$$L_2'=\sqrt{(X+\delta_X)^2+(Y+\delta_Y)^2+(Z_o+Z_c-\delta_Z)^2}.$$

Since δ_X, δ_Y and δ_Z are very small,

$$a_o(X+\delta_X, Y+\delta_Y, Z_o+\delta_Z)\approx a_o(X, Y, Z_o). \tag{11}$$

Then,

$$\begin{aligned}I'(x,y)&=a_o{}^2(X, Y, Z_o)+a_r{}^2(X_r, Y_r, Z_r)\\&\quad+2a_o{}^2(X, Y, Z_o)a_r{}^2(X_r, Y_r, Z_r)\cdot\cos[k'((L_1+L_2)-(R_{lr}+R_{cr}))].\end{aligned} \tag{12}$$

The image intensity obtained by subtracting the image before deformation from

that after deformation is,

$$\begin{aligned} I_{sub}(x,y) &= I'(x,y) - I(x,y) \\ &= -4a_o(X, Y, Z_o)a_r(X_r, Y_r, Z_r) \\ &\quad \cdot \sin\left[\frac{1}{2}(k'(\sqrt{{L_1}^2+2{L_1}''^2+{\delta_L}^2}+\sqrt{{L_2}^2+2{L_2}''^2+{\delta_L}^2}-(R_{lr}+R_{cr})) \right. \\ &\quad \left. +k((L_1+L_2)-(R_{lr}+R_{cr})))\right] \\ &\quad \cdot \sin\left[\frac{1}{2}(k'(\sqrt{{L_1}^2+2{L_1}''^2+{\delta_L}^2}+\sqrt{{L_2}^2+2{L''}_2{}^2+{\delta_L}^2}-(R_{lr}+R_{cr})) \right. \\ &\quad \left. -k((L_1+L_2)-(R_{lr}+R_{cr})))\right], \end{aligned} \tag{13}$$

where,

$$\begin{aligned} &{\delta_L}^2 = {\delta_X}^2+{\delta_Y}^2+{\delta_Z}^2, \\ &{L''}_1{}^2 = X\delta_X+Y\delta_Y-(Z_l+Z_o)\delta_Z, \quad \text{and,} \\ &{L''}_2{}^2 = X\delta_X+Y\delta_Y-(Z_o+Z_c)\delta_Z. \end{aligned}$$

δ_L is very small, and L_1 and L_2 are much larger than ${L_1}''$ and ${L_2}''$, respectively. $I_{sub}(x, y)$ is approximated to the following form,

$$\begin{aligned} I_{sub}(x,y) &\approx -4a_o(X, Y, Z_o)\ a_r(X_r, Y_r, Z_r) \\ &\quad \cdot \sin\left[\frac{1}{2}\left(k'+k)((L_1+L_2)-(R_{lr}+R_{cr}))+k'\left(\frac{{L_1}''^2}{L_1}+\frac{{L_2}''^2}{L_2}\right)\right)\right] \\ &\quad \cdot \sin\left[\frac{1}{2}\left(k'\left(\frac{{L_1}''^2}{L_1}+\frac{{L_2}''^2}{L_2}\right)+(k'-k)((L_1+L_2)-(R_{l\,r}+R_{cr})\right)\right]. \end{aligned} \tag{14}$$

A macroscopic average of $I_i(x,y)(=(I_{sub}(x,y)^2)$ is given by the following form,

$$\langle I_i(x,y)\rangle = 8{a_o}^2(X, Y, Z_o){a_r}^2(X_r, Y_r, Z_r)\cdot \sin^2\left[\frac{k}{2}p(X, Y, Z_o, \delta_X, \delta_Y, \delta_Z)\right], \tag{15}$$

where,

$$\begin{aligned} &k'' = \frac{k'}{k}, \quad \text{and} \\ &p(X, Y, Z_o, \delta_X, \delta_Y, \delta_Z) = k''\left(\frac{{L_1}''^2}{L_1}+\frac{{L_2}''^2}{L_2}\right) \\ &\qquad\qquad +(k''-1)((L_1+L_2)-(R_{lr}+R_{cr})). \end{aligned} \tag{16}$$

$\langle I_i(x,y)\rangle$ is dark in areas where $p(X, Y, Z_o, \delta_X, \delta_Y, \delta_Z)=m\lambda$ $(\lambda=0, 1, 2, \cdots)$ is satisfied, while $\langle I_i(x,y)\rangle$ is bright in areas where $p(\ )=(m+\frac{1}{2})\lambda$ $(m=0, 1, 2, \cdots)$ is satisfied. In the extreme case when the laser light is approximated to be parallel $(X, Y\approx 0)$, and $k''=1$, then $p(\ )$ is expressed by,

$$p(\ ) = -2\delta_Z. \tag{17}$$

Equation (17) holds to a fairly good approximation in this measurement system. If the wavelength of the laser light was to change $(k\neq 1)$, coaxial circular fringes would occur. But, it is assumed that thermal changes in the borehole are small and that the wavelength does not change. In this case, the system can measure quantitatively the displacement of the borehole wall in terms of the wavelength of the laser light. The sensitivity of the system will increase to measure 1/10 of the wavelength by detailed

analysis. Thus, it will be able to measure displacements smaller than 0.1 μm.

3. Results of Laboratory Tests

Laboratory tests of the system have been carried out at a basement room of the laboratory in Kyoto University.

An aluminum cylinder (inner diameter : 100 mm, thickness : 1 mm) was used as a dummy borehole. After the system was fixed in the cylinder, one surface side of the cylinder was fixed to a rigid wall in the laboratory and the opposite side was pushed by a micrometer (Figure 5(a)). The cylinder was thus deformed. The micrometer was than retracted from the cylinder surface, and the reference image of the cylinder was taken by the video camera. Subsequent images were stored in memories by using the image processor at every 1 second. An example of images processed by the image processor is shown in Figure 6. Because the object plane of the cylindrical area was taken

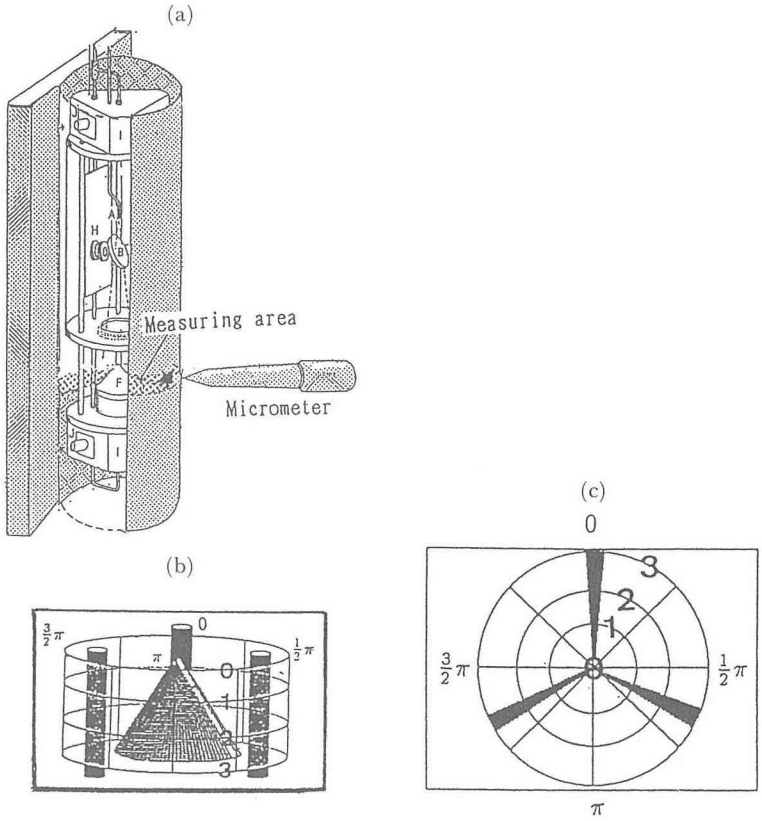

Fig. 5. (a) Layout of a laboratory test. An aluminum cylinder is employed to be a dummy borehole. Tests were performed by measuring displacements of the cylinder surface. The star denotes the point on which the micrometer was attached to push the cylinder. (b) Illustration of the cylindrical area in a borehole to be measured by the ESPI image processing system. (c) A circular image to be taken by a video camera.

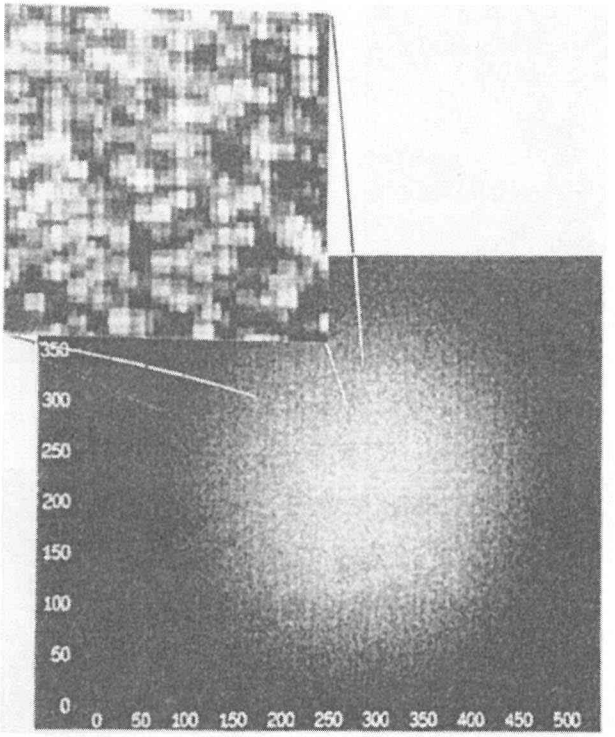

Fig. 6. An Example of speckle pattern.

by the video camera through a cone mirror (Figure 5(b)), the object plane is presented by a circle, in which the upper end of the measured area is located at the center of the circle and the lower one is the circumference of the image (Figure 5(c)). Three pillars of the measurement unit are represented by dark radial lines on the image. Therefore, the areas shadowed with the pillars could not be measured by this system.

Figure 7 shows images indicating an absolute value of the differences between the reference image and respective ones after 1, 2, 3 and 4 seconds. The mark "B" denotes the point that had been pushed by the micrometer. Patterns corresponding to the deformations of the cylindrical wall indicate that the largest deformation of the cylindrical wall occurred at B. Three dark lines indicated as the mark "A" in Figure 7 correspond to three pillars. These lines don't show the deformation of the wall. In Figure 8, images representing cylindrical deformations are shown in the same way as those in Figures 5(b) and 7. In the procedure to transform the circular image into the cylindrical one, the laser light is assumed to be parallel. In Figure 8, arrows on the top of the cylindrical wall show the directions of the deformation. In shaded areas, the radial displacement dr is,

$$-\frac{\lambda}{2}<dr<0.$$

In the areas that are covered with coarse oblique lines, dr is,

$$0<dr<\frac{\lambda}{2}.$$

In the areas that are covered with fine oblique lines, dr is,

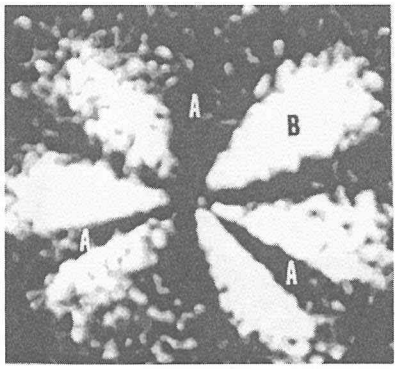

(a) An image obtained from the difference between the reference image and that after 1 seconds.

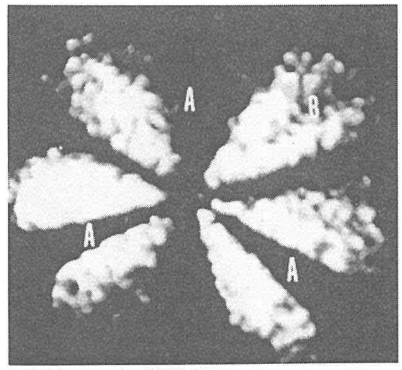

(b) An image obtained from the difference between the reference image and that after 2 seconds.

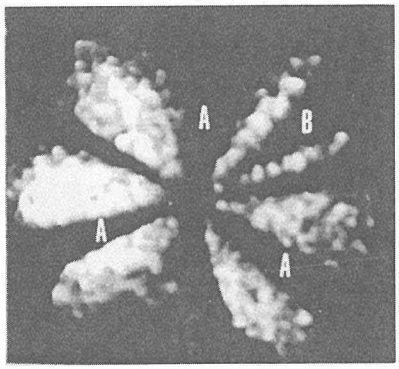

(c) An image obtained from the difference between the reference image and that after 3 seconds.

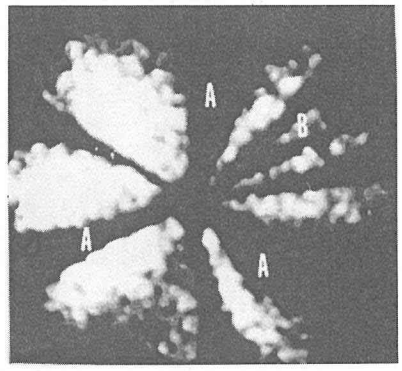

(d) An image obtained from the difference between the reference image and that after 4 seconds.

Fig. 7. Examples of results obtained from laboratory tests. A fringe corresponding to the deformation of the inner wall of the cylinder was obtained from the difference between the reference image (t=0 sec.) and respective images taken after 1, 2, 3 and 4 seconds. Three dark lines indicated by the mark 'A' correspond to three pillars where the displacement could not be detected. The mark 'B' denotes the point that had been pushed by the micrometer.

$$\frac{\lambda}{2} < dr < \lambda.$$

4. Field Experiments at Hiraki Mine

Field experiments using this measurement system were carried out at Hiraki mine in January 1993. The purposes of the experiments were to evaluate the mechanism of fixing the measurement module to a borehole wall and to check the performance of the total system. Before the start of experiments, it became clear that the diameter of the module (104 mm) was too large to be used in the overcoring procedure with a diameter of 150 mm. Moreover, the module was not waterproof. Because of these two reasons the overcoring experiment was not carried out.

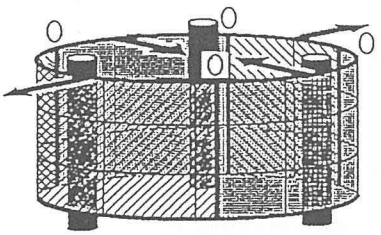

(a) The deformation during 1 second after the reference image was taken.

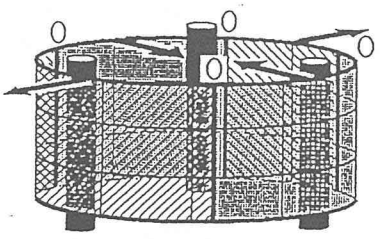

(b) The deformation during 2 second after the reference image was taken.

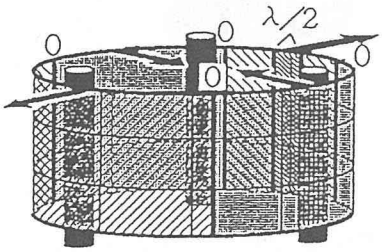

(a) The deformation during 3 second after the reference image was taken.

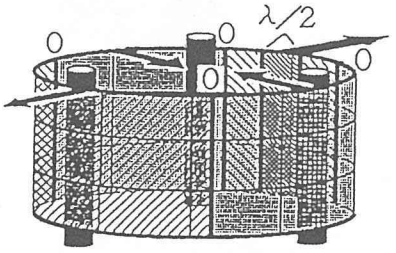

(b) The deformation during 4 second after the reference image was taken.

$-\lambda/2 < dr < 0$, $0 < dr < \lambda/2$, $\lambda/2 < dr < 2\lambda/2$

Fig. 8. Images representing cylindrical deformations in cases shown in Fig. (a)–(d). ($\lambda = 0.633\,\mu$m).

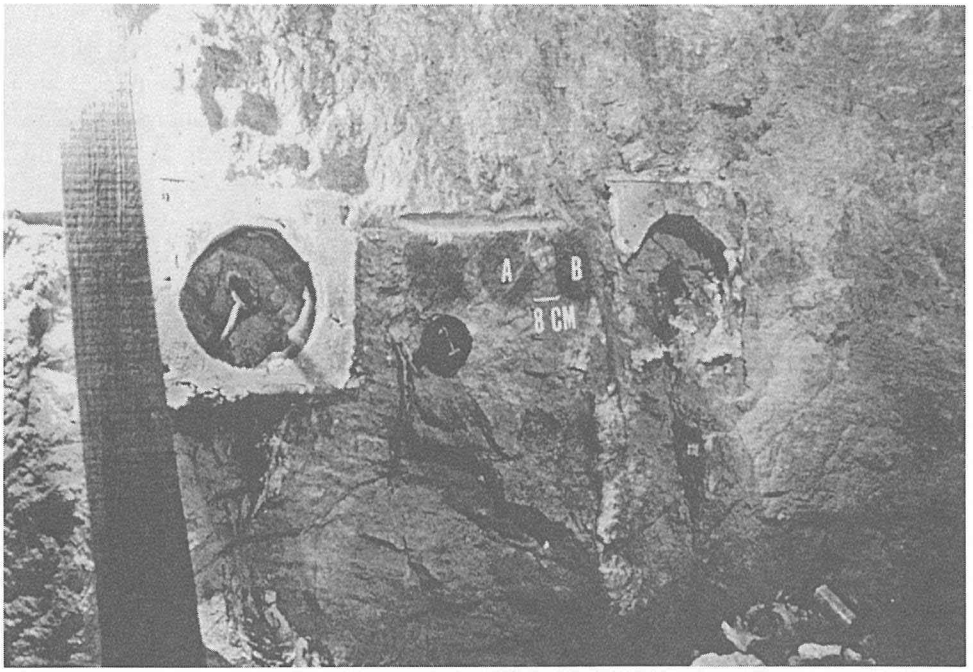

Fig. 9. View of the experiment field at Hirali mine. 'A' and 'B' denote the points where the first and second boreholes were drilled, respectively.

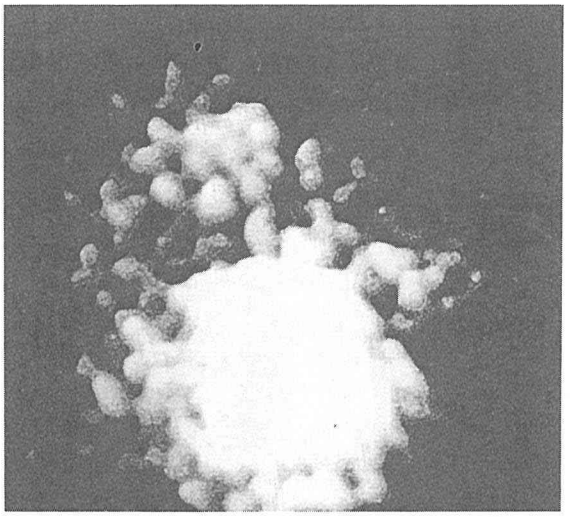

Fig. 10. An example of fringe patterns obtained by field experiments at Hiraki mine.

Figure 9 shows a layout of the experiments. A borehole with a diameter of 110 mm was first drilled into the rock's wall at the point (A) and the module was set up in this borehole. Next, a borehole B with the same diameter was drilled at the point (B) about 80 mm apart from the borehole A. Using the measurement system, radial displacements caused by the effect of drilling a new borehole were investigated.

While the boring was in progress, images were taken by the video camera and recorded every minute on a hard disk through a personal computer. After the drilling, images were recorded over the rest 12 hours.

While it was possible in the laboratory to obtain fringes over a period of 24 hours from the same reference image, continuous fringes could not be obtained in this field experiments. The reason for this failure may be twofold : Slight motions of the optical fiber would lead to loss of coherence and that the intensity of the images was very weak. Figure 10 shows an example of the images representing the radial displacement obtained in field experiments at Hiraki mine.

Consequently, we must solve some problems before the system can become field worthy, e.g. waterproofing, solving optical fiber problem, and using a very high quality video camera to enhance fringe contrast.

5. Improvement of the Measurement Module

Under the necessity of miniaturization, the measurement module was improved and a new one was manufactured. Figure 11(a) shows a schematic diagram of the new borehole module and Figure 11(b) is the view of this module. The video camera (A) is a BELL TEX 902 CCD camera unit which has 512×582 pixels. The minimum illumination required to get images through the camera is 0.2 lux. The plate (G) is the reference plane. The lens (B) is fastened with a C mount, and easily be replaced if desired. Arrangements of the video camera and the beam expander (C) are modified.

The legs (D) are interchangeable and can be set at an arbitrary length.

Modifications and features of the module are as follows. The module is divided

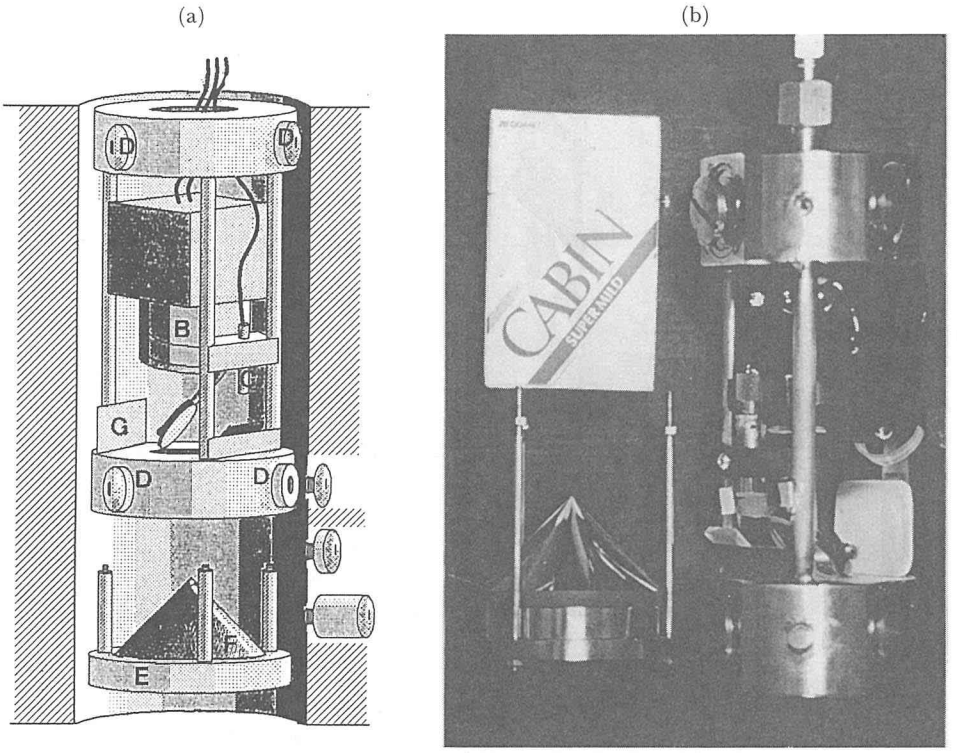

Fig. 11. (a) Schematic diagram of an improved module of the measurement system. (b) View of the module.

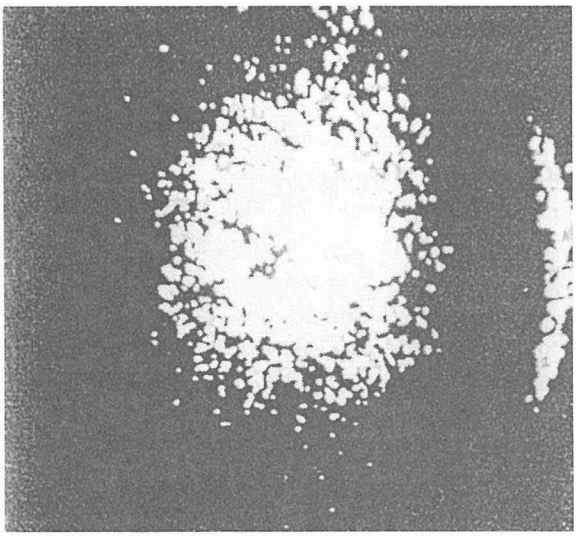

Fig. 12. An example of images measured with the improved module.

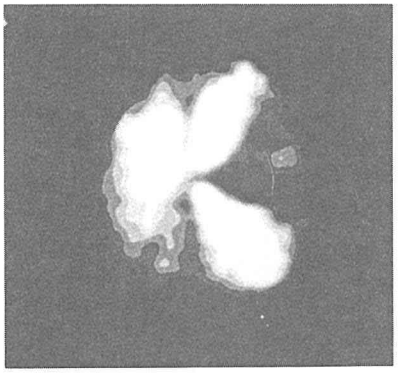

(a) An image obtained from the difference between the reference image and that after 1 second.

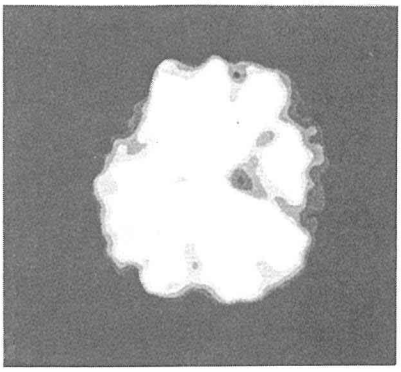

(b) An image obtained from the difference between the reference image and that after 2 seconds.

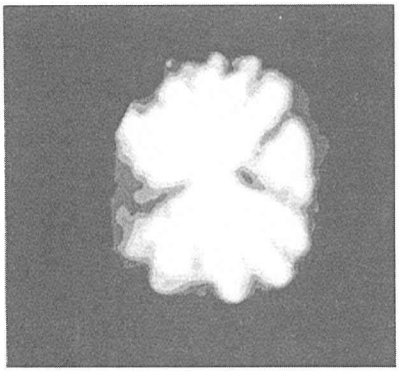

(c) An image obtained from the difference between the reference image and that after 3 seconds.

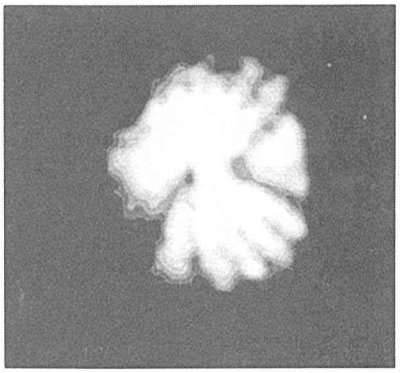

(d) An image obtained from the difference between the reference image and that after 4 seconds.

Fig. 13. Examples of laboratory tests by employing the improved module.

into two pieces; an upper and lower pieces (E). The cone mirror (F) is fixed on the lower piece. The height of the upper piece is 160 mm and its diameter is 70 mm, whereas the height of the lower piece is 70 mm. The weights of both pieces are 1.9 kg and 0.5 kg, respectively. The module is capable to measure deformation of a borehole with a diameter larger than 75 mm.

Although the original module could only be used to measure radial displacement of the surrounding cylindrical area, the improved module can also be used to measure the deformation of the bottom of the borehole.

Figure 12 shows an example of images measured in the bottom area. Figure 13 shows examples of the laboratory experiments with the improved measurement module. It shows thermal deformations of a chloroethylene cylinder (inner diameter: 78 mm, thickness: 6 mm) in the direction of the radius of the cylinder.

6. Discussion

A He-Ne laser source is too large to be used within the measurement module of the

ESPI borehole stressmeter. It is inevitable to adopt an optical fiber in the present system when using a He-Ne laser. In this case, the fiber must be long enough so as to transmit a laser beam from the source to the measurement module. It is difficult to keep the long optical fiber at a constant state for a long time during and after boring. It is thus difficult to measure displacements because of the instability of the optical system. In extreme cases, the fringes do not occur, and it is almost impossible to analyze the images. If the images were taken closely in time, it could be possible to be solved to some extent. However, when the images are taken at very short intervals, the measurements are inaccurate, since the displacements are too small to cause well defined fringes. A small-sized semiconductor laser can generate higher power than a He-Ne laser. If a semiconductor laser is used as the light source, it is not necessary to use an optical fiber. But the problem in employing a semiconductor laser as the light source in an ESPI system is that the stability of a semiconductor laser is much worse than that of the He-Ne laser at this time. It needs to be kept at a constant temperature and the electric current must be well regulated in order to stabilize the wavelength. This problem will be solved in the near future if frequency-stabilized semiconductor lasers can be used.

In measurements of the surrounding cylindrical area, the occurrence of dark lines, which are not clearly distinguishable from fringes, can't be avoided in the present design. When many fringes occur in one image, it is difficult to analyze the displacements. If images are taken frequently in a short interval and fringes are recognized in the images, displacements will be obtained from the following equation,

$$p(X, Y, Z_o, \delta_X, \delta_Y, \delta_Z)=\frac{2}{k}\ \arcsin\ \sqrt{\frac{\langle I_i(x,y)\rangle}{8a_o{}^2(X, Y, Z_o)a_r{}^2(X, Y, Z_r)}}. \quad (18)$$

Values of $p(\ )$ are discontinuous because they are obtained by an inverse trigonometric function. It is necessary to connect them continuously.

If displacements are small ($\ll\frac{1}{2}$ wavelength) within the time interval of

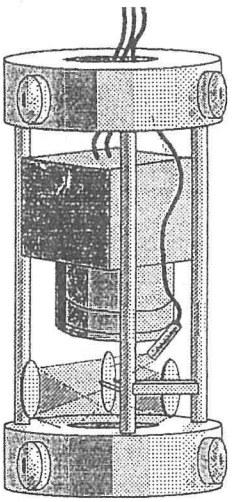

Fig. 14. An optical arrangement for measurement of in-plane displacements.

measurements, phase-shifting ESPI can be utilized, and the semiconductor laser provided can keep the wavelength under control. The phase-shifting ESPI uses three or more interference fringe patterns that are in the same deformation state but at different interference phases. A phase value at each pixel point can be determined from intensities of the different phase-shifted interference fringe patterns at the same location. The deformation of an object surface is estimated from the phase value. A measurement of the deformation is independent of the dark lines in this estimation.

It will also be possible to measure in-plane displacements by modifying the optical arrangement of the module. Figure 14 shows an optical arrangement for measurements of in-plane displacements. In this arrangement, displacements in the direction of the Y-axis can be measured, and Equation (16) is rewritten as the following equation,

$$\begin{aligned} p(\,) &= k''\left(\frac{X\delta_X+(Y_{fc}+Y)\delta_Y-Z_o\delta_Z}{L_1}-\frac{X\delta_X-(Y_{fc}-Y)\delta_Y-Z_o\delta_Z}{L_2}\right) \\ &\quad +(k''-1)(L_1-L_2) \\ &\quad L_1=\sqrt{X^2+(Y_{fc}+Y)^2+Z_o{}^2}, \quad \text{and,} \\ &\quad L_1=\sqrt{X^2+(Y_{fc}-Y)^2+Z_o{}^2} \end{aligned} \tag{19}$$

Equation (19) is approximated with the following equation in the same way as Equation (17).

$$p(\,)=\frac{2Y_{fc}}{\sqrt{2Y_{fc}{}^2+Z_o{}^2}}, \tag{20}$$

where, Z_o is the distance from a focal point of the fiber lens (A) to the object plane, and Y_{fc} is a sum of the distance from the center of the focal point of the fiber lens (A) to a mirror (B) and the distance from the center of the object to the mirror (B) in the direction of Y-axis.

7. Concluding Remarks

The Electronic Speckle Pattern Interferometry (ESPI) technique was introduced to crustal stress and strain measurements. We developed the borehole stress-strain measurement system employing ESPI. The system was designed to be able to measure out-of-plane dispacements of the wall and bottom areas of a borehole. It would also be possible to measure in-plane displacements in both areas by modifying the optical arrangement of the measurement module. The system is small-sized in due consideration of mobility and easiness of setting up. At this stage, it is difficult to measure continuosly the deformation by using the optical fibers. By employing a frequency stabilized semiconductor laser, this difficulty will be overcome.

As another application of ESPI system in geophysical sciences, we propose to employ the ESPI system in precise measurements of tunnel deformation. Measurements of crustal deformation using a laser holographic method in a deep tunnel have been carried out (TAKEMOTO, 1986, TAKEMOTO and YAMADA, 1989). In the similar manner as those, by using ESPI system, measurements of tunnel deformation in terms of the wavelength of the laser light system should be possible.

The improved module is able to measure the deformation of a tunnel without

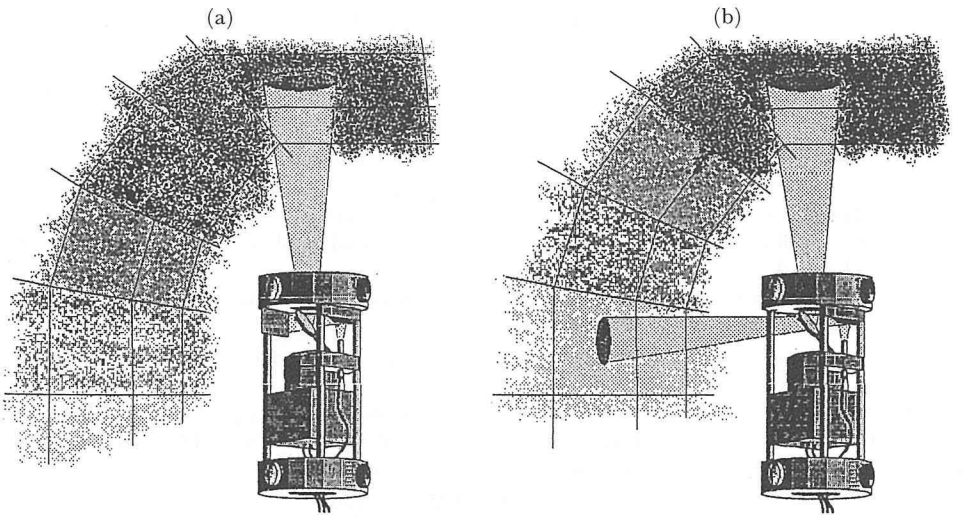

Fig. 15. Layout of precise measurements of tunnel deformations. (a) Measurement of vertical deformation. (b) Measurement of difference between vertical and horizontal deformations.

modification (Figure 15(a)). Differences between out-of-plane displacement on a side wall and the displacement on a ceiling could be measured by modifying the reference plane (Figure 15(b)). In this case, the deformation is able to be measured with high resolution because of a phase difference between the deformation in the horizontal direction and that in the vertical direction.

Acknowledgements

The authos would like to express sincere thanks for encouragement of Professors Yutaka TANAKA and Ichiro NAKAGAWA of Kyoto University. The authors are also grateful to Professor Hartmut SPETZLER of University of Colorado at Boulder and Dr. Koji TENJINBAYASHI of Mechanical Engineering Laboratory for many critical comments. The authors were favored to have the cooperation of Mr. Tsutomu Io of Io Mamufactory and Mr. Uzaburo MAGARI of Kyoto University who contributed their experimental skill to manufacture the measurement module.

This research was partially supported by the Grant-in-Aid for Scientific Research from the Ministry of Education, Science and Culture of Japan (No. 03554010) and the 19th Nissan Science Foundation.

References

BASS, J.D., SCHMITT, D. and AHRENS, T.J., Holographic *In Situ* Stress Measurements, *Geophys. J. R. astr. Soc.*, **85**, 13–41, 1986.

CHENGYONG, W., PEIDE, L., RONGSHENG, H. and XIUTANG, S., Study of the Fracture Process Zone in Rock by Laser Speckle Interferometry, *Int. J. Rock Mech. Min. Sci. & Geomech.*, **27**, 65–69, 1990.

HIRAMATSU, Y. and OKA, Y., Analysis of Stresses around a Circular Shaft or a Drift Excavated in Ground in a Three-Dimensional State, *J. Min. Metal. Inst. Japan,* **78**, 93–98, 1962.

ISHII, H., MATSUMOTO, S., HIRATA, Y., YAMAUCHI, T., TAKAHASHI, T., SUZUKI, K., WATANABE, S., WAKASUGI, T., KATO, T. and NAKAO, S., Development of New Multi-Component Small Borehole Strainmeter and Observation, *Abstr. 1992 Japan Earth Planet. Sci. Joint Meet.*, 205, 1992.

KAMEOKA, Y., Investigations on the *In Situ* Stress Measurements by the Technique of Relieving the Stress on the Bottom of a Borehole, Dr. Thesis, Kyoto Univ. 111 p, 1978.

MASTIN, L., Effect of Borehole Deviation on Breakout Orientations, *J. Geophys. Res.*, **93**, 9187–9195, 1988.

OKA, Y., KAMEOKA, Y., SAITO, T. and HIRAMATSU, Y., Investigations on the New Method of Determining Rock Stress by the Stress Relief Technique and Applications of This Method, *Rock Mech. Japan*, **3**, 68–70, 1979.

TAKEMOTO, S., Laser Interferometer Systems for Precise Measurements of Ground-Strains, *Bull. Disas. Prev. Res. Inst., Kyoto Univ.*, **29**, 65–81, 1979.

TAKEMOTO, S., Application of Laser Holographic Techniques to Investigate Crustal Deformations, *Nature*, **322**, 49–51, 1986.

TAKEMOTO, S. and YAMADA, M., Crustal Strain Measurements Using a Laser Holographic Method at the Iwakura Observatory, *Annuals, Disas. Prev. Res. Inst., Kyoto Univ.*, **32**, 75–81, 1989.

TANAKA. Y., Crustal Stress Measurements in Japan—Research Trends and Problems—, *Proceedings of Earthquake Prediction Reaearch Symposium* 1987, 199–211, 1987.

TANAKA, Y., FUJIMORI, K. and TAKEUCHI, T., Crustal Stress Measurement at the Hiraki Mine, the Hoden Quarry and the Tsuchihashi Mine in Northwest Kinki District, *Annuals, Disas. Prev. Res. Inst., Kyoto Univ.*, **33**, 23–37, 1990.

YAMAGUCHI, I., A Laser-Speckle Strain Gauge, *J. Phys. E: Sci. Instrum.*, **14**, 1270–1273, 1981.

YANAGISAWA, M., Crustal Strain Measurements Using Resistive Strain Gauge—Laboratory and Field Experiments—, *J. Geod. Soc. Japan*, **30**, 274–286, 1984.